Response of the East Asian Winter Monsoon to Strong Tropical Volcanic Eruptions

JIAPENG MIAO

Nansen-Zhu International Research Center, Institute of Atmospheric Physics, Chinese Academy of Sciences, Beijing, and Nanjing University of Information Science and Technology, Nanjing, and College of Earth Science, University of Chinese Academy of Sciences, Beijing, China

TAO WANG AND YALI ZHU

Nansen-Zhu International Research Center, Institute of Atmospheric Physics, and Climate Change Research Center, Chinese Academy of Sciences, Beijing, China

JINZHONG MIN

Nanjing University of Information Science and Technology, Nanjing, China

HUIJUN WANG

Nansen-Zhu International Research Center, Institute of Atmospheric Physics, and Climate Change Research Center, Chinese Academy of Sciences, Beijing, and Nanjing University of Information Science and Technology, Nanjing, China

DONG GUO

Climate Change Research Center, Chinese Academy of Sciences, Beijing, China

(Manuscript received 26 August 2015, in final form 19 April 2016)

ABSTRACT

In this study, a 600-yr integration performed with the Bergen Climate Model (BCM), version 2.0, was used to investigate the impact of strong tropical volcanic eruptions (SVEs) on the East Asian winter monsoon (EAWM). It is found that SVEs have an important influence on the East Asian winter climate. The volcanic forcing can cause changes in surface heat fluxes and tropospheric circulation, particularly over the tropics and high-latitude regions. As a result, Arctic Oscillation enters into its positive phase in the first two winters after SVEs. The associated circulation weakens the Siberian high and reduces the cold air transport to East Asia, which is not conducive to the enhancement of the EAWM during this period. At the same time, the North Pacific Ocean gradually cools and shapes La Niña–like sea surface temperature (SST) anomalies in the third winter after SVEs. The Walker circulation is strengthened over the Pacific, and two anomalous lower-tropospheric cyclones are located over the South China Sea and southeast of Japan, respectively. Therefore, related northeasterly wind anomalies appear along the East Asian coast, indicating a strengthened EAWM during this period. Meanwhile, the enhanced Siberian high and East Asian trough further contribute to the enhancement of EAWM in the third winter. It is therefore concluded that the SVEs-induced climate changes over the tropical Pacific and north polar regions play an important role in regulating the EAWM in the posteruption winters.

1. Introduction

As an important part of the East Asian monsoons, the East Asian winter monsoon (EAWM) is one of the most active systems in the boreal winter (Chen and Sun 1999).

Corresponding author address: T. Wang, 40 Hua Yan Li, Qi Jia Huo Zi, Institute of Atmospheric Physics, Chinese Academy of Sciences, Chao Yang District, Beijing 100029, China.
E-mail: wangtao@mail.iap.ac.cn

DOI: 10.1175/JCLI-D-15-0600.1

The EAWM has a direct effect on East Asian weather and climate, which is key to exploring the mechanism of climate change over East Asia (Tao and Chen 1987). Significant interannual variability of the EAWM can lead to intense snowfall, cold surge activity, and other disasters (e.g., Sun et al. 2010; H. J. Wang et al. 2012). To date, most research has revealed a declining trend of the EAWM in the future on a background of global warming, which will likely cause more extreme climate events in China (Wang and Fan 2013). Hence, from the perspective of climate change and global warming, changes in the EAWM are also a key scientific issue.

The EAWM can be affected by multiple factors and has shown a large interannual variability in the past few decades, which makes it very difficult to predict (Jia et al. 2014). Until now, more attention has been paid to the intrinsic factors in the atmosphere–ocean–sea ice system, such as sea surface temperature (SST) anomalies (Chen 2002; Li and Wang 2012; Wang and He 2012), the Antarctic Oscillation (Wang and Fan 2005), the Arctic Oscillation (AO) (Gong et al. 2001; Jhun and Lee 2004; Tan et al. 2007), jet streams (Yang et al. 2002), and Arctic sea ice anomalies (Wu and Wang 2002; Wang and Sun 2009; Liu et al. 2012). For instance, Chen (2002) notes that in the winter preceding an El Niño event anomalous northerlies occur over the East Asian region. However, anomalous southerlies appear over East Asia in the winter during the mature phase of an El Niño event. The situations for the impact of La Niña on the East Asian winter climate are approximately the reverse of but not as significant as those of El Niño. Gong et al. (2001) and Wu and Wang (2002) suggested that the winter AO directly affects sea level pressure (SLP), surface air temperature (SAT), and the 500-hPa East Asian trough over the region northward of 35°N in East Asia. Liu et al. (2012) concluded that the decline of Arctic sea ice has played a critical role in recent cold and snowy winters.

External forcings, including anthropogenic forcings (greenhouse gases and tropospheric aerosols) and natural forcings (total solar irradiance and volcanoes), can affect the global and regional climate. For instance, the rapidly increasing concentrations of atmospheric greenhouse gases have strong impacts on climate. Previous climate model experiments have suggested that the late twentieth-century warming was likely due primarily to increases in greenhouse gases (Wigley et al. 1997; Stott et al. 2000, 2001; Hegerl et al. 2007). It is also well known that high tropospheric aerosol concentrations can slow down the tropical meridional overturning circulation and decrease regional summer precipitation in South Asia (Bollasina et al. 2011). A recent study suggested that anthropogenic forcings are most likely the prime drivers of the interdecadal variation of the summer precipitation over eastern China in the late 1970s (Wang et al. 2013). In addition, simulations with coupled general circulation models (GCMs) show that solar forcing dominates over internal variability in generating temperature variations over decadal and longer time scales and large spatial scales (Cubasch et al. 1997; Drijfhout et al. 1999; Rind et al. 1999). Volcanic eruption is a vital climate forcing over seasonal-to-multidecadal time scales (Shindell et al. 2004; Gleckler et al. 2006; Emile-Geay et al. 2008), and the global mean temperature responses to the corresponding radiative forcing have been adapted as one constraint on climate system feedbacks and sensitivity (e.g., Annan and Hargreaves 2006).

Strong tropical volcanic eruptions (SVEs) can inject a large amount of volcanic aerosols into the stratosphere. In one aspect, these aerosols can reduce the downward solar radiation to cool the surface. However, they can also absorb both solar and terrestrial radiation to heat the stratosphere. Therefore, SVEs can induce short-term energy imbalances in the climate system (Stenchikov et al. 1998; Robock 2000). For instance, Kirchner et al. (1999) found that, for the 2-yr period following the eruption of Mount Pinatubo in 1991, a general cooling of the global troposphere occurred. In addition, major explosive eruptions are generally followed by an anomalously positive phase of the AO/North Atlantic Oscillation (NAO) in the two boreal winters (Groisman 1992; Robock and Mao 1992, 1995; Perlwitz and Graf 1995). As a result of positive AO/NAO, a clear winter warming pattern of the SAT usually can be found over the Northern Hemisphere continents following strong eruptions (Robock and Mao 1992; Kirchner et al. 1999). Furthermore, several GCM simulations predict that, in response to large tropical and extratropical eruptions, drought conditions appear over monsoon areas (Oman et al. 2005; Fan et al. 2009; Schneider et al. 2009); dry conditions were observed in the region following the eruption of Mount Pinatubo in 1991, although this year also corresponded to a persistent El Niño (Trenberth and Dai 2007). Recently, Cui et al. (2014) noted that both simulation and National Centers for Environmental Prediction (NCEP)–National Center for Atmospheric Research (NCAR) reanalysis data show a weakening of the East Asian summer monsoon (EASM) in strong eruption years and the model simulation suggests that northern and southern China experience droughts, and the Yangtze–Huaihe River valley experiences floods during eruption years. Similarly, Iles and Hegerl (2014) found that global monsoon rainfall was decreased following strong eruptions. A recent study also suggested that SVEs induce decadal dynamical responses in the coupled ocean–atmosphere system (Zanchettin et al.

2012), and SVEs were typically followed, after approximately one decade, by a succession of anomalously warm winters over Europe (delayed winter warming) (Zanchettin et al. 2013). In addition, volcanic eruptions can also impact the Pacific decadal oscillation (PDO) (T. Wang et al. 2012), which is a key factor affecting global and regional climate on a decadal time scale (Mantua and Hare 2002; Hegerl et al. 2007; Zhu et al. 2011).

To date, the potential relationship between the EAWM and external natural forcings has received little attention. In this study, we thus examine the response of the EAWM to SVEs using a 600-yr integration of the Bergen Climate Model (BCM), version 2.0 (Otterå et al. 2009). We describe the model and methods in section 2. In section 3, we evaluate the model performance and investigate the response of the EAWM to SVEs, as well as associated processes. Conclusions and a discussion are given in section 4.

2. Model, experiments, and methods

An advanced fully coupled atmosphere–ocean–sea ice climate model, the Bergen Climate Model, version 2 (Otterå et al. 2009), is used here to study the impacts of SVEs on the EAWM. The atmospheric component of the BCM is the ARPEGE model from Météo-France (Déqué et al. 1994), which is run at spectral T63 horizontal resolution (~2.8° × 2.8°) and employs 31 vertical levels ranging from the surface to 10 hPa. The ocean component is the Miami Isopycnic Coordinate Ocean Model (MICOM) (Bleck and Smith 1990; Bleck et al. 1992). This ocean model has a stack of 34 isopycnic layers in the vertical and an almost regular horizontal grid spacing of approximately 2.4° × 2.4°, with the exception of the equatorial region (the meridional direction is decreased to 0.8°). The sea ice component is the Global Experimental Leads and Ice for Atmosphere and Ocean (GELATO), which is a dynamic–thermodynamic sea ice model including multiple ice categories (Salas Mélia 2002). These components are coupled with the OASIS (version 2) coupler (Terray and Thual 1995). The BCM is stable for several centuries' integration without any flux adjustments.

The multiple-century simulation used here is a 600-yr integration (Otterå et al. 2010; T. Wang et al. 2012). It includes external forcings due to the changes in the amount of stratospheric aerosols following SVEs and to the variation in the total solar irradiance (TSI) for the last 600 years (Crowley et al. 2003). The other forcings are held constant at preindustrial levels. The TSI forcing field is based on a reconstruction (Lean et al. 1995) after 1610 and is provided as variations in the effective solar constant, which will in turn modify the shortwave flux at the top of the atmosphere. The volcanic aerosol optical characteristics are supplied as monthly optical depths at 0.55 μm in the middle of the visible spectrum in four bands [30°–90°N, equator–30°N, 30°S–equator, and 90°–30°S (Crowley et al. 2003)], which are converted to volcanic aerosol concentration according to Crowley (2000) and added into the model. Only the direct effect and first indirect effect of tropospheric sulfate aerosols are taken into account. Using this implementation, BCM relatively realistically simulated the main features observed after the Mount Pinatubo eruption in 1991 (Otterå 2008).

In addition, the NCEP–NCAR monthly reanalysis data (Kalnay et al. 1996) and the Climatic Research Unit (CRU) monthly datasets (Mitchell and Jones 2005) are used to examine the model performance on the EAWM.

Considering the general characteristics of the EAWM, we investigate the validity of the simulated climatology of SAT, SLP, and the 850-hPa wind field (Jiang et al. 2005; He and Wang 2012). We use the following three statistics to quantitatively assess the simulated climatology in East Asia: namely, the regional average, regional average error, and spatial correlation coefficient. These statistical variables were specifically introduced in Jiang et al. (2005).

The superposed epoch analysis (SEA) was first used to examine the effects of volcanoes on climate by Mitchell (1961). And this method has been applied in many studies since 1990s (e.g., Mass and Portman 1989; Robock 1991; Robock and Mao 1995; Adams et al. 2003). To obtain clear effects of SVEs on the East Asian winter climate, the SEA is used on the EAWM indices in this study. Additionally, a standard Monte Carlo randomization procedure is used to determine the statistical significance of the SEA (a total of 10 000 Monte Carlo simulations). We choose four categories of EAWM indices defined by Gong et al. (2001) using SLP over East Asia, by Chen et al. (2000) using low-level wind, by Cui and Sun (1999) using the 500-hPa geopotential height, and by Yan et al. (2009) using an integrated index that includes the SAT, east–west pressure gradient, and 500-hPa geopotential height. Moreover, the Niño-3 SST index, AO index, and u50 index are also used to examine the related large-scale climate changes after the SVEs. The Niño-3 SST index is defined as the normalized SST anomalies averaged over the Niño-3 area (5°S–5°N, 150°–90°W). The AO index is defined as the principal component of the first empirical orthogonal function (EOF) of the SLP anomalies over the domain poleward of 20°N. The u50 index is defined as the normalized zonal-mean zonal wind anomalies at 50 hPa over 65°N.

TABLE 1. SVE years based on Crowley et al. (2003) and winter years used for the SEA and composite analysis. The volcanic explosivity index (VEI; Krakauer and Randerson 2003) is given; 4 is large; 5 and higher are very large.

	Eruption description				
Year	Name	Latitude	Radiative forcing ($W m^{-2}$)	VEI	First winter (DJF) years after SVEs
1453	Kuwae	16.8°S	−4.2	6	1453/54
1460	Unknown	—	−1.3	—	1460/61
1586	Kelut	7.9°S	−1.3	5	1586/87
1600	Huaynaputina	16.6°S	−1.9	6	1600/01
1620	Unknown	—	−1.1	—	1620/21
1641	Mount Parker	6.1°N	−1.7	5	1641/42
1674	Mount Gamkonora	1.4°N	−1.5	5	1674/75
1680	Unknown	—	−1.1	—	1680/81
1693	Serusa	6.3°S	−1.1	4	1693/94
1809	Unknown	—	−2.9	—	1809/10
1815	Tambora	8.3°S	−5.6	7	1815/16
1831	Babuyan Claro	19.5°N	−1.3	4	1831/32
1835	Cosigüina	13.0°N	−1.4	5	1835/36
1883	Krakatau	6.1°S	−2.6	6	1883/84
1902	Santa Maria	14.8°N	−1.3	6	1902/03
1963	Mount Agung	8.3°S	−1.9	4	1963/64
1982	El Chichón	17.4°N	−2.1	5	1982/83
1991	Mount Pinatubo	15.1°N	−3.3	6	1991/92

Furthermore, a simple compositing analysis is used to examine the influence of SVEs on the East Asian winter climate, which involves sorting the data into different phases based on a ''volcanic eruption year'' for synchronization and then comparing the mean state of those phases. According to this method, we can investigate the spatial patterns of climate changes in the different posteruption winters (e.g., first winter after the eruptions, second winter after the eruptions, and so on) relative to the climatology. If given sufficient data, a common potential (causal) response to the forcing event should emerge in the average (composite), while other noises in the data should cancel. Here, we use a Student's t test method to determine the statistical significance of the compositing analysis. In this study, 18 SVEs during the last 600 years are chosen with an anomalous negative radiative forcing larger than 1 $W m^{-2}$ at the top of the atmosphere [Table 1, calculated as in Otterå et al. (2010); the aerosol loading values were converted to radiative forcing by dividing by 30 and multiplying by 23.5 (Sato et al. 1993)].

3. Results

a. *Evaluation of the model's East Asian winter climatology*

First, we examine whether the BCM can reliably reproduce the East Asian winter climatology, because this ability is directly related to the utility of this model for investigating the response of the EAWM to SVEs.

As shown in Fig. 1a, the observational winter SAT gradually decreases northward. A large extent of colder temperature appears over the Tibetan Plateau, and a small extent of warming appears over the Sichuan basin and Xinjiang Province, which are associated with topography. Figure 1b shows that the simulated distribution of SAT generally agrees with the observation. The spatial correlation coefficient is 0.93 with respect to the observation (Table 2). However, there is a large extent of warming bias in the north of China, particularly to the west of Lake Baikal (Fig. 1c). The maximum warming bias is approximately 8°C. In the whole EAWM area, the simulated regional averaged temperature is −7.74°C, which is higher by 0.57°C than the observation. These large model biases are partly caused by the different covering periods between the long-term BCM simulation and the CRU dataset.

For simulated SLP, the BCM well captures the locations of the Siberian high and Aleutian low in the wintertime (Figs. 1d,e). The spatial correlation coefficient is 0.94 with respect to the reanalysis data. However, the BCM simulates lower SLP over the Tibetan Plateau compared to the reanalysis data (Fig. 1f) but higher SLP over the Pacific. The simulated regional averaged SLP is 1023.22 hPa, higher by 0.52 hPa than the observation. Even if there are some model biases, the BCM successfully reproduces the geographical distribution of the East Asian winter SAT and SLP.

The most prominent feature of the EAWM is the northwesterly wind flowing along the eastern flank of the Siberian high that divaricates in the south of Japan,

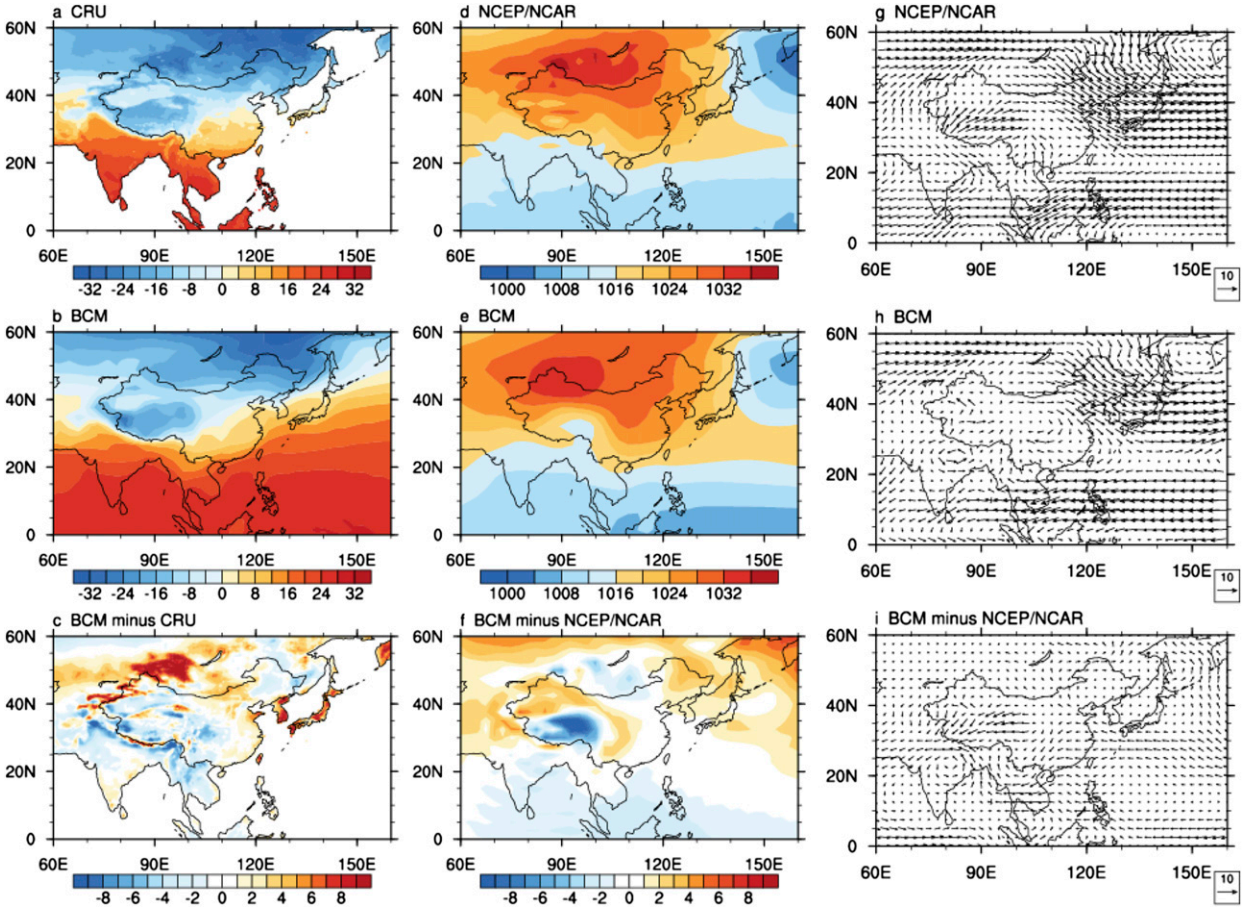

FIG. 1. Winter SAT (December–February; °C) from (a) the CRU dataset for the period of 1900–99, (b) BCM for the period of 1400–1999, and (c) BCM minus the CRU dataset. Winter SLP (hPa) from (d) the NCEP–NCAR reanalysis dataset for the period of 1948–99, (e) BCM, and (f) BCM minus NCEP–NCAR. Winter 850-hPa wind field (m s^{-1}) from (g) the NCEP–NCAR reanalysis dataset, (h) BCM, and (i) BCM minus NCEP–NCAR.

with on-branch flow straight toward the subtropical western and central Pacific and the other flowing along the coast of East Asia (Fig. 1g) (Lau and Li 1984; Chen et al. 2000). Figure 1h shows that the BCM-simulated wind field at 850 hPa coincides well with the observed spatial pattern. The spatial correlation coefficients of zonal wind, meridional wind, and wind speed between the reanalysis data and BCM are 0.97, 0.92, and 0.81, respectively. In addition, the simulated zonal wind and wind speed are a little smaller than the observation. However, the simulated meridional wind is relatively larger.

Overall, the BCM is able to reproduce the spatial pattern of the East Asian winter climate and should therefore constitute a good starting point to investigate the response of the EAWM to SVEs in the model.

b. *Response of the EAWM to SVEs*

Volcanic aerosols can directly affect Earth's radiation balance (Robock 2000). Figure 2 illustrates the results of

TABLE 2. The values of three statistics for EAWM-related meteorological elements (u_{850} is the 850-hPa zonal wind; v_{850} is the 850-hPa meridional wind; and uv_{850} is the 850-hPa horizontal wind).

	Regional average	Regional average error	Spatial correlation coefficient
Land SAT (°C) (15°–60°N, 70°–140°E)	−7.74	0.57	0.93
SLP (hPa) (15°–60°N, 70°–140°E)	1023.22	0.52	0.94
u_{850} (m s^{-1}) (10°–60°N, 115°–150°E)	0.63	−0.97	0.97
v_{850} (m s^{-1}) (10°–60°N, 115°–150°E)	−2.07	0.47	0.92
uv_{850} (m s^{-1}) (10°–60°N, 115°–150°E)	6.06	−0.17	0.81

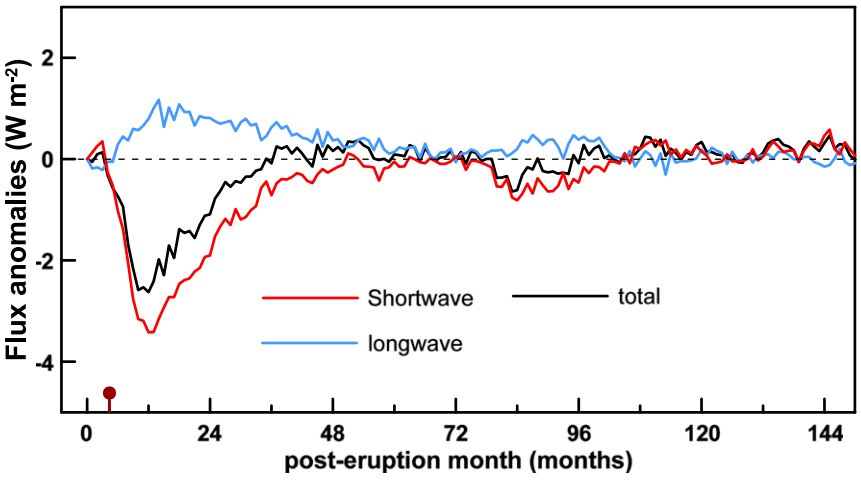

FIG. 2. SEA of simulated 18 posteruption monthly anomalies of globally averaged top-of-atmosphere radiative fluxes. Positive values denote downward flux.

the SEA on the monthly, globally averaged, top-of-atmosphere radiative flux anomalies for 18 cases of SVEs during the last 600 years in our experiment. An enormous amount of sulfur dioxide (SO_2) is ejected by SVEs, which is converted to sulfate aerosol and leads to an approximate $-3.5\,W\,m^{-2}$ maximum peak reduction of the global average downward shortwave flux because of the reflection and scattering of the incoming solar radiation by the aerosol. At the same time, by absorbing the upward longwave radiation from the troposphere and surface, the aerosol layer also reduces the global average outgoing longwave radiation, with a peak value of approximately $1\,W\,m^{-2}$. After SVEs, therefore, the total radiation decreases significantly, more than $-2.5\,W\,m^{-2}$ at the peak. This radiative climatic influence of SVEs can persist for approximately three years at the top of atmosphere.

Forced by such strong external forcing, significant climate changes can be observed in winter over East Asia in the BCM. Figure 3 illustrates the results of the SEA on the simulated EAWM indices for 18 cases of SVEs during the last 600 years in the BCM, showing the evolution of these indices following the SVEs on an annual time scale. The EAWM indices do not significantly change following the SVEs. Instead, they all increase obviously in the third winter after the SVEs. The increased SLP index suggests a strengthened Siberian high. At the same time, the increased circulation and 500-hPa geopotential height (H500) indices indicate enhanced winter circulation and a deepened East Asian trough, respectively. Besides, the EAWM integrated index also increases during this period. Therefore, according to the SEA on the different EAWM indices, particularly for the change in the EAWM integrated index, the SVEs could result in a stronger EAWM in the BCM.

To further confirm the influence of SVEs on the EAWM, we analyze the anomalies of vital atmospheric variables after eruptions. A composite analysis is applied in which anomalies are calculated by taking the variables during the third winter after the 18 SVEs and subtracting the 600-yr winter climatology. Figure 4a shows the composite anomalies of the simulated winter SAT in the third winter following the SVEs. Significant negative SAT anomalies can be found over most regions of East Asia and surrounding ocean. The strongest cooling is observed in the northern Xinjiang Province, the center of Inner Mongolia, and southern China and Indo-China. As a result of different responses of the North Pacific climate to the SVEs noted by T. Wang et al. (2012), the SAT over the northwestern Pacific Ocean decreases to a lesser extent compared to that over land, which results in an increased land–sea thermal contrast.

Though the EAWM is a regional phenomenon, its variation is well related to the change in large-scale circulation (Wang and Jiang 2004). The anomaly pattern of winter atmospheric circulation associated with the EAWM can be diagnosed in the SLP, 850-hPa wind, and H500 data. As shown in Fig. 4b, following the SVEs, higher SLP is observed over the Asian continent, and the maximum anomalies appear in the region of the Siberian high (larger than 1 hPa), implying a stronger Siberian high during this winter.

Because these 18 SVEs all occurred in the tropics, the air cooling in the troposphere is stronger over tropics

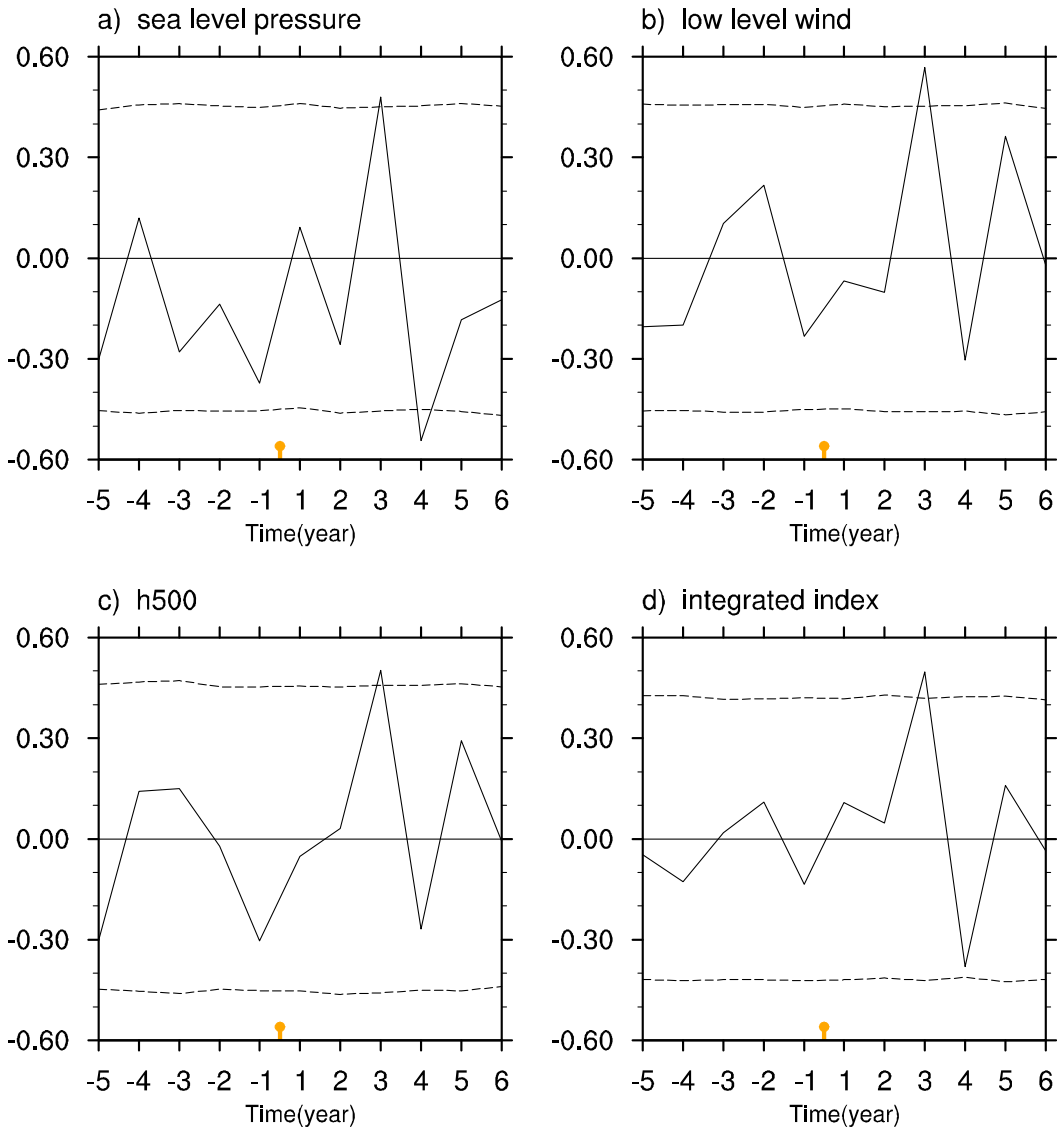

FIG. 3. SEA for the simulated EAWM indices defined by (a) sea level pressure over East Asia (Gong et al. 2001). (b) low-level wind (Chen et al. 2000), (c) 500-hPa geopotential height (Cui and Sun 1999), and (d) an integrated index (Yan et al. 2009) that includes surface air temperature, east–west pressure gradient, and 500-hPa geopotential height. Year 1 on the *x* axis is the first winter after the SVEs. The dashed lines represent confidence intervals of 95% derived from 10 000 Monte Carlo simulations.

than over the other latitudes. Thus, the H500 also decreases significantly over the tropics following the SVEs (Fig. 4c). Particularly in southern Japan, the decreased H500 reaches approximately 12 m, indicating a stronger East Asian trough following the SVEs relative to the normal winter. As a result, anomalous northerly winds are evident over East Asia, southern Japan, and the surrounding ocean (Fig. 4d). Additionally, these anomalous northerly winds bring higher-latitude cold air to the lower latitude, which contributes to the surface cooling over East Asia mentioned above. At the same time, a cyclonic anomaly can be observed over Southeast Asia. It is also indicated that the EAWM circulation is significantly strengthened after the SVEs. Moreover, the precipitation is increased over the South China Sea (Fig. 4e), whereas it is decreased over the middle and lower reaches of the Yangtze River valley and in Japan and the Korea Peninsula.

c. *Possible mechanism for the response*

As shown in Fig. 3, the EAWM indices are strengthened significantly in the third winter, rather than immediately

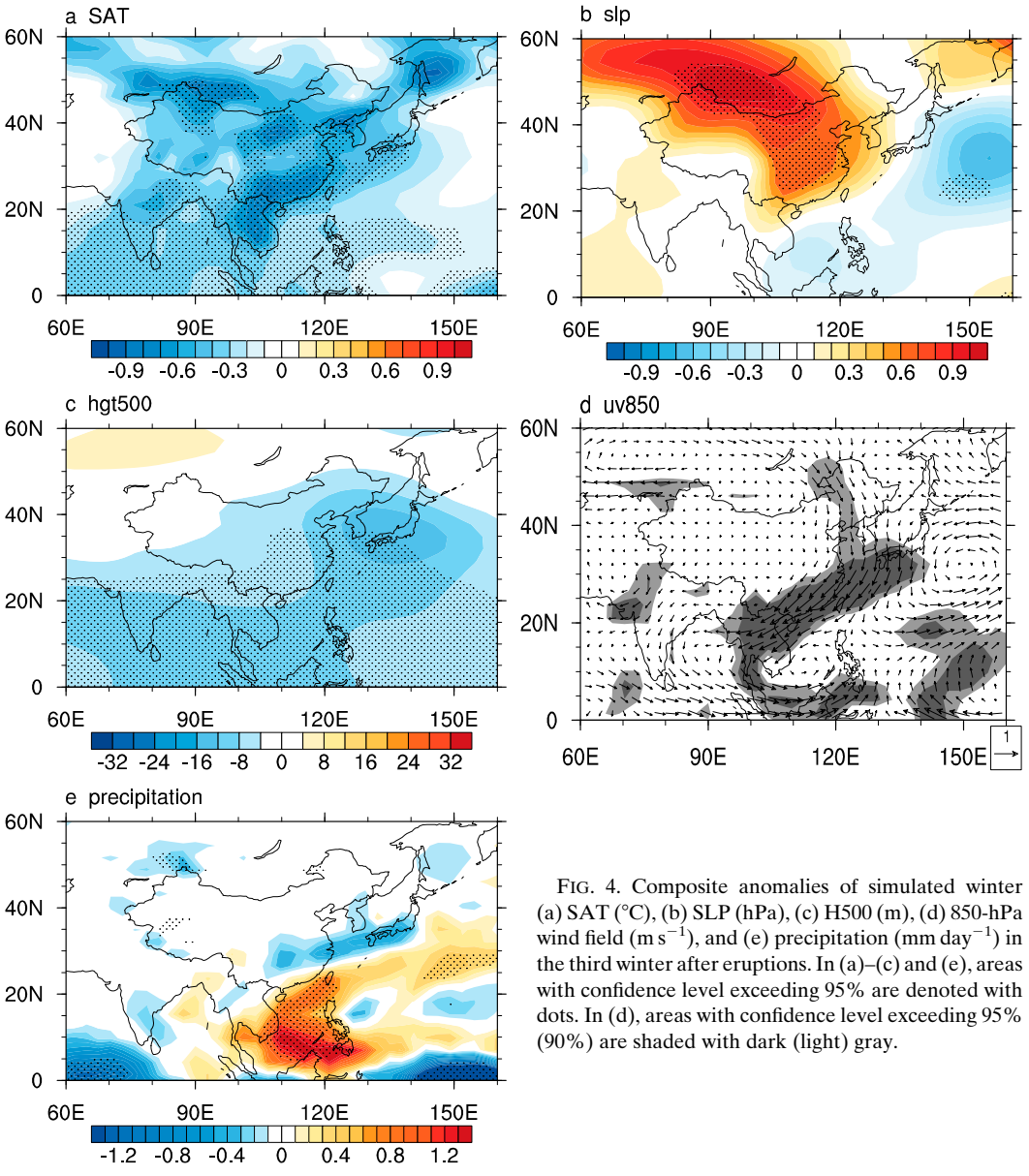

FIG. 4. Composite anomalies of simulated winter (a) SAT (°C), (b) SLP (hPa), (c) H500 (m), (d) 850-hPa wind field (m s^{-1}), and (e) precipitation (mm day^{-1}) in the third winter after eruptions. In (a)–(c) and (e), areas with confidence level exceeding 95% are denoted with dots. In (d), areas with confidence level exceeding 95% (90%) are shaded with dark (light) gray.

following the SVEs. To understand the mechanism behind the response of the EAWM, we examine the associated climate changes over East Asia and the North Pacific in each winter following the SVEs.

Figure 5 illustrates the response of North Pacific SST to the SVEs during different periods. In the first winter after the SVEs, the western and eastern tropical SSTs and the Bering Sea start cooling (Fig. 5a). Then significant negative SST anomalies are evident over the central extratropical North Pacific and the western tropical Pacific (Fig. 5b). Nevertheless, positive SST anomalies are observed on the equator around the international date line and develop into El Niño–like SST pattern in the second winter. These weak warmings are surrounded by the negative SST anomalies, which are mainly caused by the volcanic cooling effect. In the third winter, significant negative SST anomalies appear over the tropics, instead of the previous weak warming over the central-eastern tropical Pacific. This anomalous SST pattern strongly resembles the cold phase of ENSO (i.e., La Niña event; Fig. 5c). Unlike normal La Niña events, the tropical negative SST anomalies even extend to the western Pacific warming pool in the third winter after the SVEs. At the same time, positive SST anomalies are evident over the midlatitude northwestern Pacific. The SEA of the Niño-3 SST index further confirms the

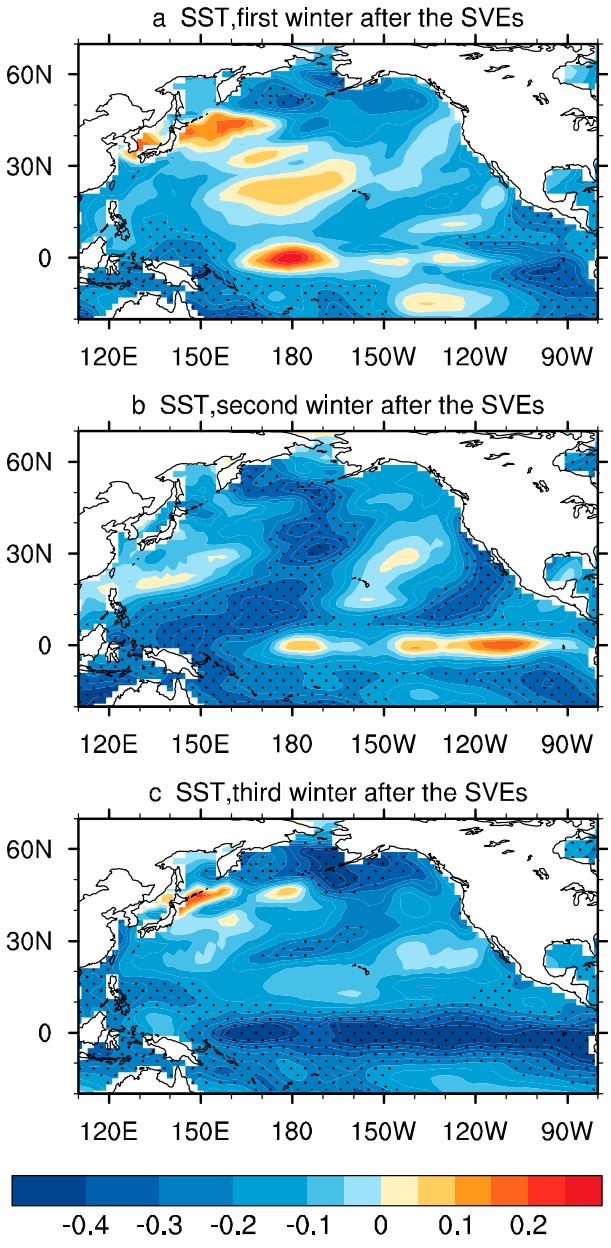

FIG. 5. The composite anomalies of SST (°C) for the (a) first, (b) second, and (c) third winter after the SVEs. Areas with confidence level exceeding 95% are denoted with dots.

evolution of tropical Pacific SSTs following the SVEs. The negative signal is significant in the third winter after the SVEs (Fig. 6a), indicating a La Niña event. But it is hard to find any El Niño signals in SST anomalies in the first two winters because of the dominant volcanic cooling effect over tropics. However, narrow positive SST anomalies over the central-eastern tropical Pacific still suggest an El Niño event in the second winter following the SVEs. Similar responses of the ENSO cycle to the SVEs can also be found in the observations (Liu et al. 2015), long-term reconstructed data (Adams et al. 2003), and multimodel results from phase 5 of the Coupled Model Intercomparison Project (Maher et al. 2015). And yet the related mechanism is still unclear and needs further investigation.

There is a close relationship between El Niño or La Niña events and variability of the EAWM (e.g., Zhou et al. 2007, 2013; Yang and Jiang 2014). As shown in Figs. 7a and 7b, the regression maps of atmospheric circulation on the Niño-3 index reveal that, during the El Niño events, anomalous westerly winds in the lower troposphere and anomalous easterly winds in the upper troposphere are observed over the tropical central Pacific, implying a weakened Walker circulation over the tropics and a suppressed convection over the warm pool. These changes are mainly induced by the tropical central-eastern Pacific warming during this period. At the same time, the opposite circulation anomalies, including anomalous easterly winds in the lower troposphere and anomalous westerly winds in the upper troposphere, are evident over the Maritime Continent. Because of the anomalous circulation over the tropical western Pacific, significant southwesterly wind anomalies can be found over Indo-China and southern China. This means that the EAWM is often weakened during the El Niño events. On the contrary, the EAWM is strengthened during the La Niña events. This type of teleconnection between the ENSO cycle and the Asian winter circulation has also been documented based on an observational study (Wang et al. 2000; Chang et al. 2004).

Similarly, SVEs-induced anomalous SST over the tropics can lead to overlying anomalous circulation. As shown in Figs. 8a and 8b, upward motion is enhanced around the international date line in the first two winters after the SVEs, which is mainly caused by the tropical central Pacific warming (Figs. 5a,b). Besides, El Niño–like SST anomalies also weaken the downward motion over the tropical eastern Pacific in the second winter. This kind of anomalous circulation over the tropical Pacific is not conducive to the enhancement of EAWM during this period, as mentioned above. Differently, the La Niña–shaped SST anomalies lead to more significant circulation changes in the third winter, particularly over the tropical western Pacific. In the lower troposphere, westerly and easterly wind anomalies are evident over the Maritime Continent and tropical warm pool, respectively (Fig. 7c). This suggests that there is an anomalous low-level convergence at approximately 130°E over the tropics (Fig. 7e). In the upper troposphere, corresponding, opposite circulation anomalies can be found over the tropical western Pacific (Fig. 7d), indicating an anomalous high-level divergence around the Maritime

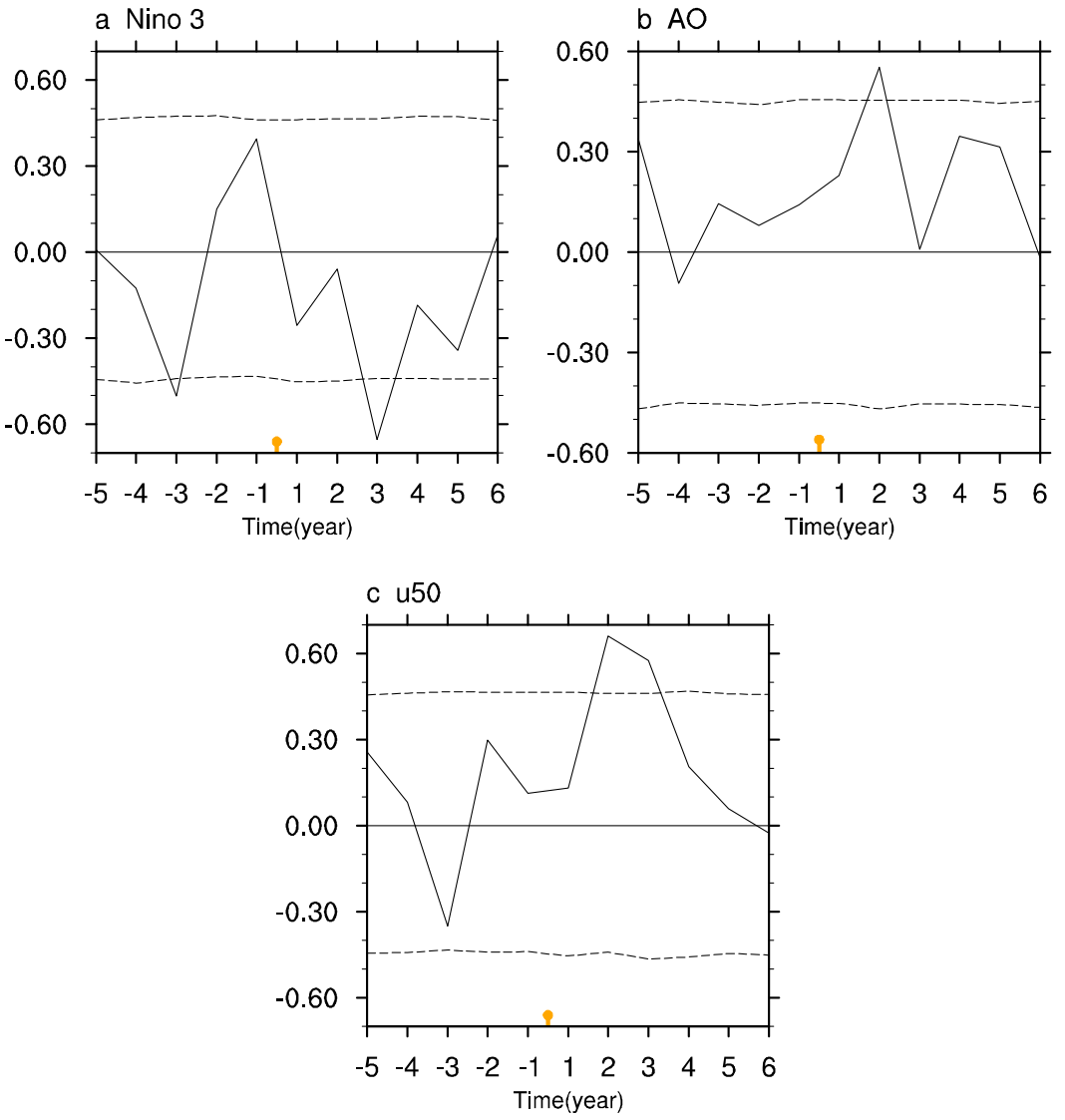

FIG. 6. SEA for the simulated wintertime series of normalized indices for (a) the Niño-3 SST index, (b) the AO index, and (c) the zonal-mean zonal wind at 50 hPa over 65°N. Year 1 on the *x* axis is the first winter after the SVEs. The dashed lines represent confidence intervals of 95% derived from 10 000 Monte Carlo simulations.

Continent (Fig. 7f). The upward motion is enhanced significantly west of 130°E (Fig. 8c). These anomalous circulations resemble the above regression maps when the La Niña events occur. However, the anomalous convection is more westward compared to the regression maps. This is likely caused by the more westward extension of the tropical, cooled SST in the third winter than that during the normal La Niña events (Fig. 5c). In addition, two related anomalous low-level cyclones can be found over the South China Sea and southeast of Japan, respectively (Figs. 7c,e). As a result, anomalous northeasterly winds appear along the East Asian coast, indicating a strengthened EAWM. These two anomalous low-level cyclones become the key bridge linking the tropical SST anomalies and the EAWM, as noted by Wang et al. (2000). Therefore, the La Niña–shaped SST anomalies in the third winter after the SVEs can contribute to the enhancement of EAWM.

At the same time, the local Hadley cell over the subtropical Asian region is strengthened (Fig. 9a) because of the enhanced convection over the South China Sea and the Maritime Continent (Figs. 7e,f). Correspondingly, the related midlatitude cell over East Asia is also strengthened (Fig. 9a). Thus, anomalous low-level divergence and high-level convergence can be observed over northern East Asia. As a result, the Siberian high is enhanced during this period, as shown in Fig. 4b. On the

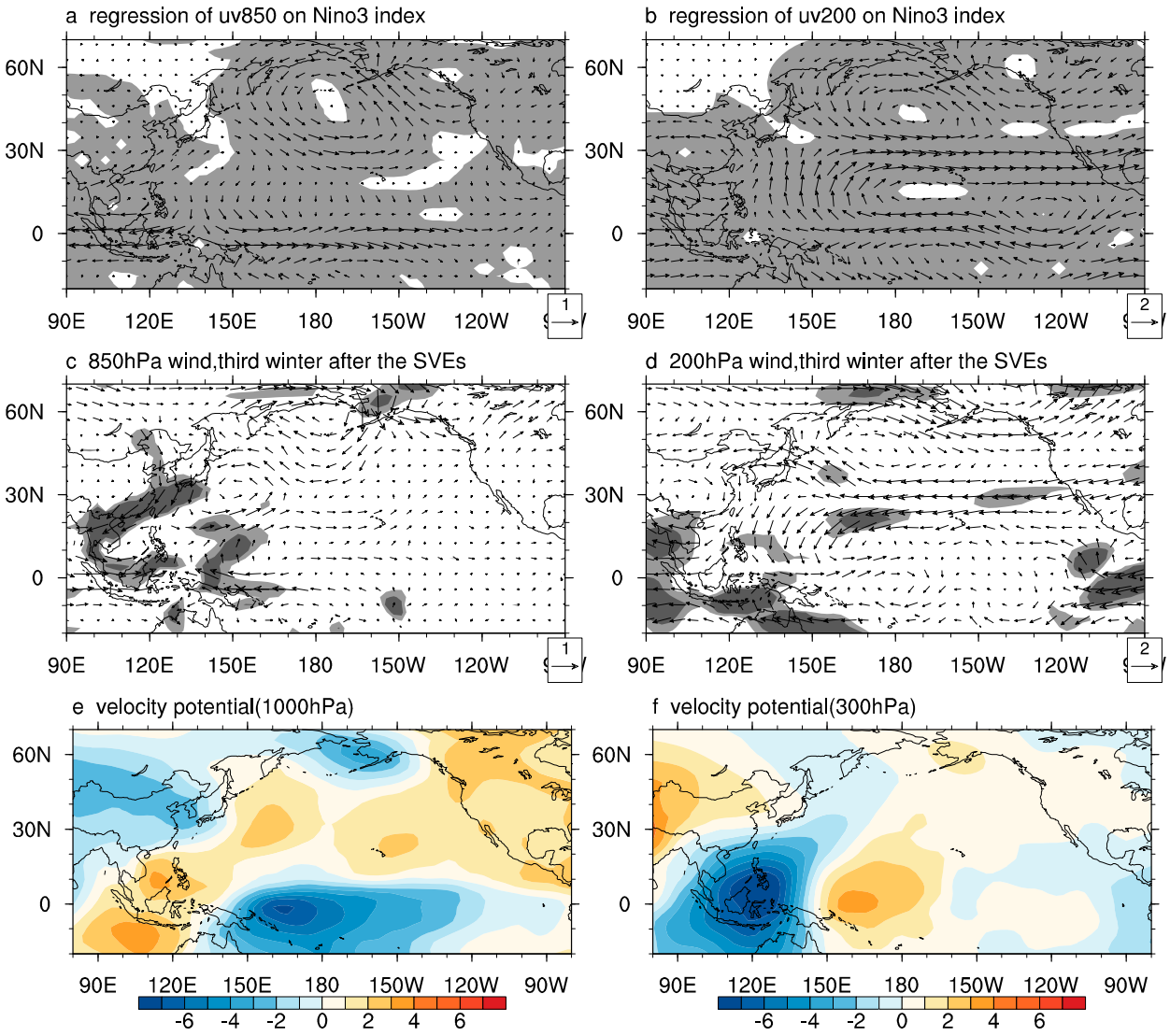

FIG. 7. Regression of simulated winter (a) 850-hPa wind (m s^{-1}) and (b) 200-hPa wind (m s^{-1}) on time series of the Niño-3 SST index for the period of 1400–1999. Composite anomalies of simulated winter (c) 850-hPa wind field (m s^{-1}), (d) 200-hPa wind field (m s^{-1}), (e) 1000-hPa velocity potential (10^5 m^2 s^{-1}), and (f) 300-hPa velocity potential (10^5 m^2 s^{-1}) in the third winter after eruptions. In (a)–(d), areas with confidence level exceeding 95% (90%) are shaded with dark (light) gray.

other hand, all of the tropospheric air is cooled over the Siberian region (Fig. 9b) as a result of negative surface radiation fluxes (not shown). As noted by Ding et al. (1991), this region is very important for the development of the Siberian high, and the overlying cooled troposphere is able to contribute to a stronger high pressure center there. Therefore, the combined effects of the convergence at middle and high levels and the surface radiative cooling play a dominant role in strengthening the Siberian high in the third winter after the SVEs, which can further contribute to the enhancement of the EAWM.

Moreover, these La Niña–shaped SST anomalies can also lead to stronger atmosphere cooling and declining geopotential height over the tropics, which can deepen the East Asian trough (Fig. 4c) and also contribute to the stronger EAWM in the third winter.

Overall, the SVE-induced La Niña–shaped SST anomalies and associated circulation anomalies contributed to a stronger EAWM in the third winter. However, why does the response of the EAWM to the SVEs not occur immediately after the eruptions? In the following section, more attention will be paid to this issue.

d. Explanation for delayed response

SVEs can induce short-term (1–2 yr) energy imbalances in the climate system (Fig. 2). However, the

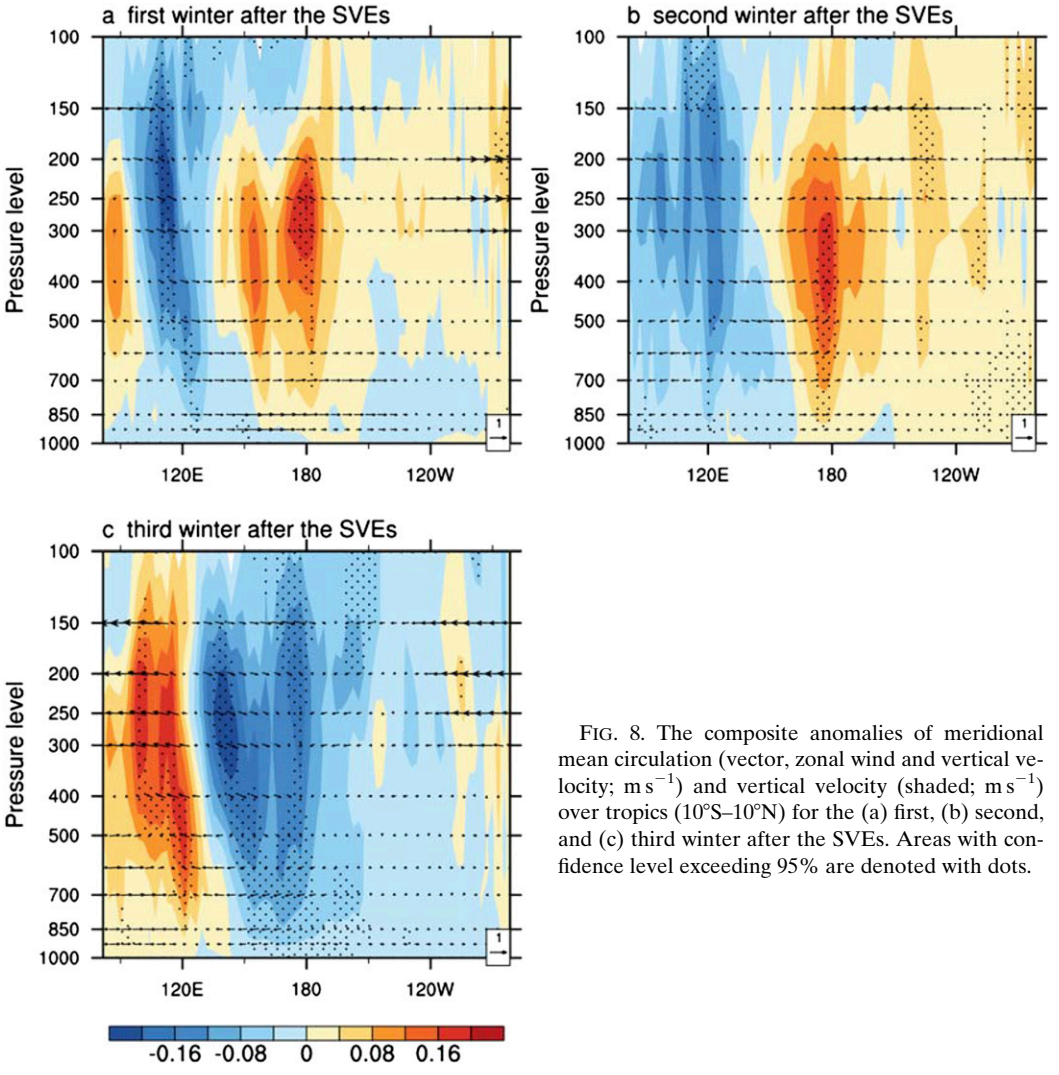

FIG. 8. The composite anomalies of meridional mean circulation (vector, zonal wind and vertical velocity; m s^{-1}) and vertical velocity (shaded; m s^{-1}) over tropics (10°S–10°N) for the (a) first, (b) second, and (c) third winter after the SVEs. Areas with confidence level exceeding 95% are denoted with dots.

EAWM indices do not change immediately following the SVEs (Fig. 3). Instead, they increase obviously in the third winter after the SVEs. To understand the mechanism behind the delayed response of the EAWM, it is necessary to examine the corresponding atmospheric circulation variability in the first two years.

Figure 10 illustrates the evolution of Northern Hemisphere SLP after the SVEs. After the SVEs, negative SLP anomalies are present over the Arctic region that subsequently and gradually expand to the northern region of the continents. They are surrounded by the positive SLP anomalies, particularly in the second winter after the SVEs, showing an anomalously positive AO pattern. The SEA of the AO index further confirms this response. The AO index is maximized in the second winter (Fig. 6b), which is consistent with changes in the stratospheric polar vortex (Fig. 6c). Its root cause is the SVE-enhanced pole-to-equator temperature gradient (e.g., Robock 2000; Otterå 2008). Typically, the interannual variability of the EAWM is closely related to changes in the AO and north polar vortex (Gong et al. 2001; Jhun and Lee 2004; Chen and Kang 2006). Consistent with the observational study (Chen and Kang 2006), the positive AO and enhanced polar vortex can lead to a northward shift of the East Asian westerly jet stream (Figs. 11a,b) and weaken the northerly winds over East Asia (Fig. 11a) in the second winter following the SVEs. At the same time, the North Atlantic Oscillation enters into its positive phase resulting from changes in the AO and polar vortex (Fig. 10). Correspondingly, enhanced westerly winds blowing across the Atlantic bring more moist and warm air into northern Europe (Fig. 11a). Additionally, cold air from the polar region is reduced over northern Eurasia due to northward polar jet. Therefore, a winter warming can be observed over high-latitude regions in Europe and western Russia (Fig. 11d) in the second winter after

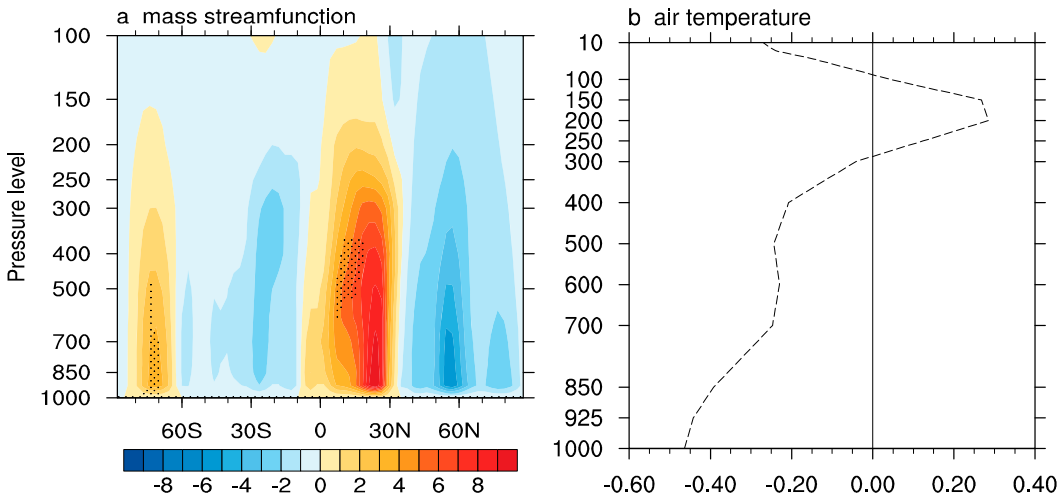

FIG. 9. (a) Composite anomalies of simulated meridional mass streamfunction (along 90°E; 10^{10} kg s^{-1}) during the third winter after eruptions; areas with confidence level exceeding 90% are denoted with dots. (b) The vertical distribution of air temperature anomalies (°C) averaged over the key region for Siberian high development (42.5°–57.5°N, 80°–120°E) during the third winter after eruptions.

the SVEs, similar to reported findings (Fischer et al. 2007; Hegerl et al. 2011). As a result, negative SLP anomalies are evident over the Siberian region, suggesting a weakened Siberian high. Thus, changes of SLP and low-level winds contribute to weaken the EAWM in the second winter following the SVEs (Figs. 3a,b). On the other hand, most regions of East Asia are cooled by the negative volcanic radiation fluxes (Fig. 11d). They also lead to negative geopotential height anomalies (insignificant) at 500 hPa

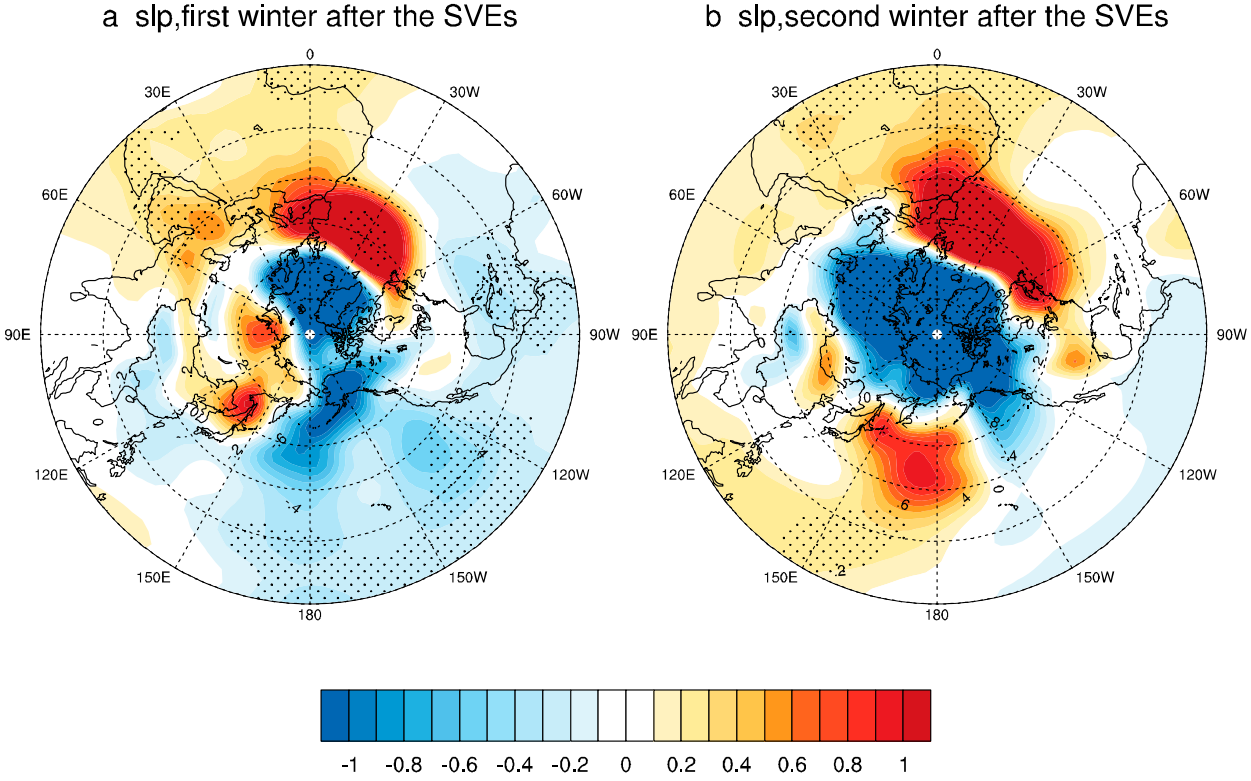

FIG. 10. The composite anomalies of SLP (hPa) for the (a) first and (b) second winter after the eruptions. Areas with confidence level exceeding 95% are denoted with dots.

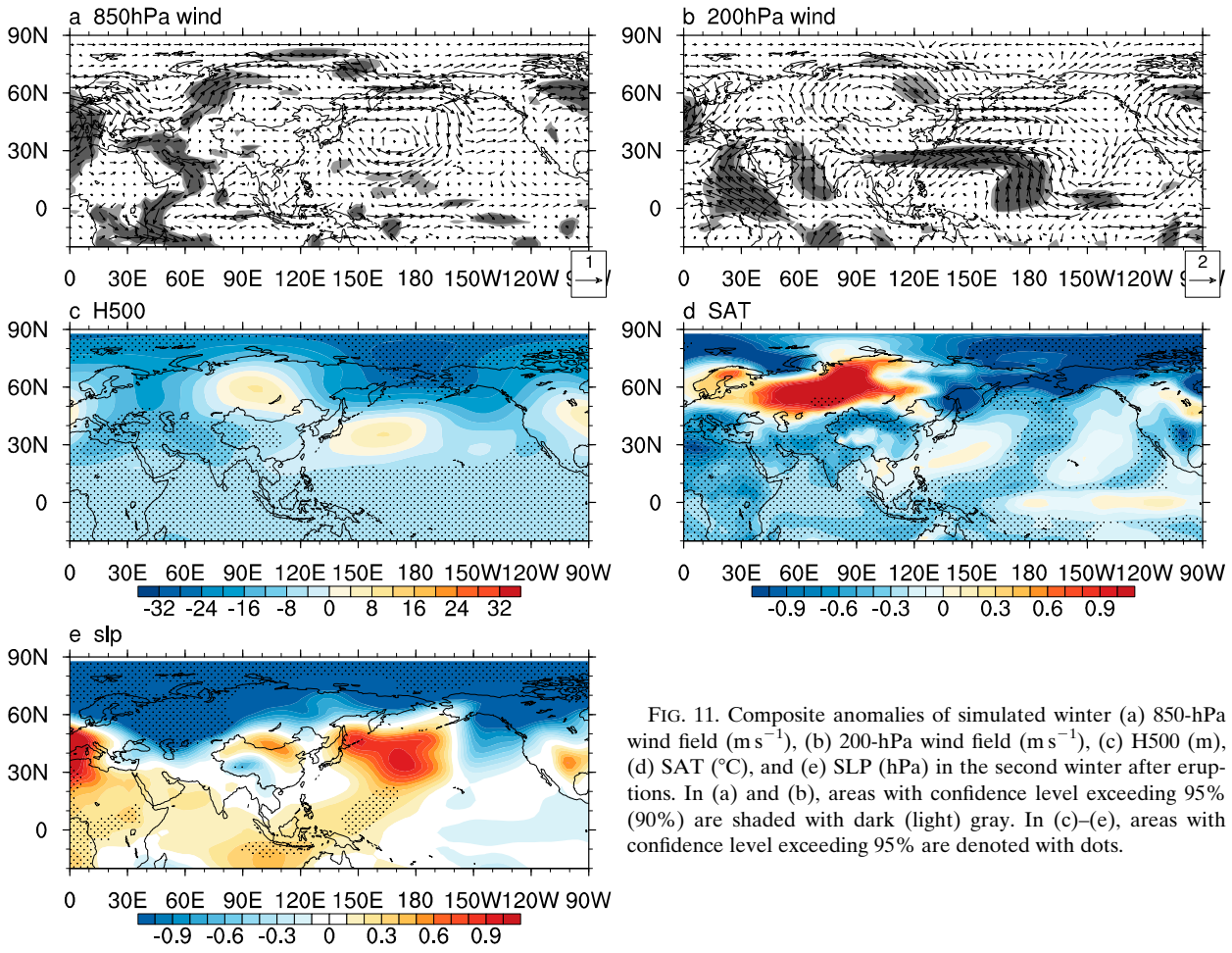

FIG. 11. Composite anomalies of simulated winter (a) 850-hPa wind field ($m\,s^{-1}$), (b) 200-hPa wind field ($m\,s^{-1}$), (c) H500 (m), (d) SAT (°C), and (e) SLP (hPa) in the second winter after eruptions. In (a) and (b), areas with confidence level exceeding 95% (90%) are shaded with dark (light) gray. In (c)–(e), areas with confidence level exceeding 95% are denoted with dots.

over the east coast of the continent, implying an enhanced East Asian trough (Fig. 11c). This could have led to a strengthened EAWM. Nevertheless, the integrated index for the EAWM changes little (Fig. 3d) because of offsetting contributions from different factors (Siberian high, northerly winds, East Asian trough, and temperature). Therefore, the SVE-induced positive AO weakens the impacts of SVEs on the EAWM in the first two winters, which explains the delayed enhancement of the EAWM following the SVEs.

4. Conclusions and discussion

The paper investigates the responses of the EAWM to SVEs in the BCM, version 2.0. The model can simulate the winter climatology realistically in multiple meteorological factors, such as the SAT, SLP, and 850-hPa wind field. However, some model biases still exist. For example, the BCM simulates a higher SAT over north of China and a lower SLP over the Tibetan Plateau compared to the observations.

Four categories of EAWM indices all indicate that a strengthened winter monsoon is observed over East Asia in the third winter following the SVEs. The simulated changes in the SAT, SLP, H500, and wind fields at 850 hPa are examined during this period. The enhanced Siberian high and East Asian winter trough, as well as anomalous northerly winds over East Asia, further confirm a stronger EAWM following the SVEs in the BCM. The SVE-induced La Niña–shaped SST anomalies and associated circulation anomalies play an important role in strengthening the EAWM in the third winter after the eruptions. On the contrary, the positive AO and enhanced polar vortex caused by the SVEs are not conducive to the formation of the strong EAWM during the first two winters as a result of a weakening of the Siberian high and northerly winds from higher latitudes to East Asia. Therefore, the EAWM becomes stronger in the third winter, rather than immediately following the SVEs.

In the observation, there are only three SVEs (i.e., the Mount Agung eruption in 1963, El Chichón eruption in

1982, and Mount Pinatubo eruption in 1991) in the past 60 years. Therefore, it is difficult to identify the direct relationship between changes of the EAWM and the SVEs because of the small sample size of SVEs in the observations and the complex impacts from other external forcings (such as greenhouse gases and anthropogenic aerosols) on the EAWM. On the other hand, whether the BCM-simulated linkage between SVEs and EAWM can be reproduced by other models need further investigation.

To date, observational and model studies both indicate that SVEs can have a large short-term impact on climate. Additionally, SVEs can also lead to long-term climate changes through their influence on the ocean's heat content, sea level, and oceanic advections (Church et al. 2005; Hansen et al. 2005; Stenchikov et al. 2009; T. Wang et al. 2012; Zanchettin et al. 2012). Here, we focused on only the short-term response of the EAWM to the SVEs. Whether the long-term impacts of SVEs on the ocean can further influence the EAWM should be addressed in the future.

Acknowledgments. We sincerely thank the three anonymous reviewers and Dr. John Chiang for their helpful comments and suggestions on the earlier versions of the manuscript. The authors are grateful to Odd Helge Otterå for providing the model simulation data. This research was supported by the National Basic Research Program of China (2012CB955401), the strategic technological program of the Chinese Academy of Sciences (XDA05090405), and the National Natural Science Foundation of China (Grant 41575086, Grant 41205051, and Grant 41205054).

REFERENCES

Adams, J. B., M. E. Mann, and C. M. Ammann, 2003: Proxy evidence for an El Niño–like response to volcanic forcing. *Nature*, **426**, 274–278, doi:10.1038/nature02101.

Annan, J. D., and J. C. Hargreaves, 2006: Using multiple observationally-based constraints to estimate climate sensitivity. *Geophys. Res. Lett.*, **33**, L06704, doi:10.1029/2005GL025259.

Bleck, R., and L. T. Smith, 1990: A wind-driven isopycnic coordinate model of the north and equatorial Atlantic Ocean: 1. Model development and supporting experiments. *J. Geophys. Res.*, **95**, 3273–3285, doi:10.1029/JC095iC03p03273.

——, C. Rooth, D. Hu, and L. T. Smith, 1992: Salinity-driven thermocline transients in a wind- and thermohaline-forced isopycnic coordinate model of the North Atlantic. *J. Phys. Oceanogr.*, **22**, 1486–1505, doi:10.1175/1520-0485(1992)022<1486:SDTTIA>2.0.CO;2.

Bollasina, M. A., Y. Ming, and V. Ramaswamy, 2011: Anthropogenic aerosols and the weakening of the South Asian summer monsoon. *Science*, **334**, 502–505, doi:10.1126/science.1204994.

Chang, C. P., Z. Wang, J. Ju, and T. Li, 2004: On the relationship between western maritime continent monsoon rainfall and ENSO during northern winter. *J. Climate*, **17**, 665–672, doi:10.1175/1520-0442(2004)017<0665:OTRBWM>2.0.CO;2.

Chen, J., and S. Q. Sun, 1999: East Asian winter monsoon anomaly and variation of global circulation. Part I: A comparison study on strong and weak winter monsoons (in Chinese). *Chin. J. Atmos. Sci.*, **23**, 101–111.

Chen, W., 2002: Impacts of El Niño and La Niña on the cycle of the East Asian winter and summer monsoon (in Chinese). *Chin. J. Atmos. Sci.*, **26**, 595–610.

——, and L. H. Kang, 2006: Linkage between the Arctic Oscillation and winter climate over East Asia on the interannual timescale: Roles of quasi-stationary planetary waves (in Chinese). *Chin. J. Atmos. Sci.*, **30**, 863–870.

——, H. F. Graf, and R. H. Huang, 2000: The interannual variability of East Asian winter monsoon and its relation to the summer monsoon. *Adv. Atmos. Sci.*, **17**, 48–60, doi:10.1007/s00376-000-0042-5.

Church, J. A., N. J. White, and J. M. Arblaster, 2005: Significant decadal-scale impact of volcanic eruptions on sea level and ocean heat content. *Nature*, **438**, 74–77, doi:10.1038/nature04237.

Crowley, T. J., 2000: Causes of climate change during the last 1000 years. *Science*, **289**, 270–277, doi:10.1126/science.289.5477.270.

——, S. K. Baum, K.-Y. Kim, G. C. Hegerl, and W. T. Hyde, 2003: Modeling ocean heat content changes during the last millennium. *Geophys. Res. Lett.*, **30**, 159–171, doi:10.1029/2003GL017801.

Cubasch, U., R. Voss, G. C. Hegerl, J. Waszkewitz, and T. J. Crowley, 1997: Simulation of the influence of solar radiation variations on the global climate with an ocean–atmosphere general circulation model. *Climate Dyn.*, **13**, 757–767, doi:10.1007/s003820050196.

Cui, X. P., and Z. B. Sun, 1999: East Asian winter monsoon index and its variation analysis (in Chinese). *J. Nanjing Inst. Meteor.*, **22**, 321–325.

Cui, X. D., Y. Gao, and J. Sun, 2014: The response of the East Asian summer monsoon to strong tropical volcanic eruptions. *Adv. Atmos. Sci.*, **31**, 1245–1255, doi:10.1007/s00376-014-3239-8.

Déqué, M., C. Dreveton, A. Braun, and D. Cariolle, 1994: The ARPEGE/IFS atmosphere model: A contribution to the French community climate modelling. *Climate Dyn.*, **10**, 249–266, doi:10.1007/BF00208992.

Ding, Y. H., S. G. Wen, and Y. J. Li, 1991: A study of dynamic structures of the Siberian high in winter (in Chinese). *Acta Meteor. Sin.*, **49**, 430–439.

Drijfhout, S. S., R. J. Haarsma, J. D. Opsteegh, and F. M. Selten, 1999: Solar-induced versus internal variability in a coupled climate model. *Geophys. Res. Lett.*, **26**, 205–208, doi:10.1029/1998GL900277.

Emile-Geay, J., R. Seager, M. A. Cane, E. R. Cook, and G. H. Haug, 2008: Volcanoes and ENSO over the past millennium. *J. Climate*, **21**, 3134–3148, doi:10.1175/2007JCLI1884.1.

Fan, F. X., M. E. Mann, and C. M. Ammann, 2009: Understanding changes in the Asian summer monsoon over the past millennium: Insights from a long-term coupled model simulation. *J. Climate*, **22**, 1736–1748, doi:10.1175/2008JCLI2336.1.

Fischer, E. M., J. Luterbacher, E. Zorita, S. F. B. Tett, C. Casty, and H. Wanner, 2007: European climate response to tropical volcanic eruptions over the last half millennium. *Geophys. Res. Lett.*, **34**, L05707, doi:10.1029/2006GL027992.

Gleckler, P. J., T. M. Wigley, B. D. Santer, J. M. Gregory, K. AchutaRao, and K. E. Taylor, 2006: Volcanoes and climate: Krakatoa's signature persists in the ocean. *Nature*, **439**, 675–675, doi:10.1038/439675a.

Gong, D. Y., S. W. Wang, and J. H. Zhu, 2001: East Asian winter monsoon and Arctic Oscillation. *Geophys. Res. Lett.*, **28**, 2073–2076, doi:10.1029/2000GL012311.

Groisman, P. Y., 1992: Possible regional climate consequences of the Pinatubo eruption: An empirical approach. *Geophys. Res. Lett.*, **19**, 1603–1606, doi:10.1029/92GL01474.

Hansen, J., and Coauthors, 2005: Earth's energy imbalance: Confirmation and implications. *Science*, **308**, 1431–1435, doi:10.1126/science.1110252.

He, S. P., and H. J. Wang, 2012: Analysis of the decadal and interdecadal variations of the East Asian winter monsoon as simulated by 20 coupled models in IPCC AR4 (in Chinese). *Acta Meteor. Sin.*, **26**, 476–488, doi:10.1007/s13351-012-0407-6.

Hegerl, G., and Coauthors, 2007: Understanding and attributing climate change. *Climate Change 2007: The Physical Science Basis*, S. Solomon et al., Eds., Cambridge University Press, 665–745.

——, J. Luterbacher, F. Gonza'lez-Rouco, S. F. B. Tett, and T. J. Crowley, 2011: Influence of human and natural forcing on European seasonal temperatures. *Nat. Geosci.*, **4**, 99–103, doi:10.1038/ngeo1057.

Iles, C. E., and G. C. Hegerl, 2014: The global precipitation response to volcanic eruptions in the CMIP5 models. *Environ. Res. Lett.*, **9**, 104012, doi:10.1088/1748-9326/9/10/104012.

Jhun, J. G., and E. J. Lee, 2004: A new East Asian winter monsoon index and associated characteristics of the winter monsoon. *J. Climate*, **17**, 711–726, doi:10.1175/1520-0442(2004)017<0711:ANEAWM>2.0.CO;2.

Jia, X., H. Lin, and X. Yao, 2014: The influence of tropical Pacific SST anomaly on surface air temperature in China. *J. Climate*, **27**, 1425–1444, doi:10.1175/JCLI-D-13-00176.1.

Jiang, D. B., H. J. Wang, and X. M. Lang, 2005: Evaluation of East Asian climatology as simulated by seven coupled models. *Adv. Atmos. Sci.*, **22**, 479–495, doi:10.1007/BF02918482.

Kalnay, E., and Coauthors, 1996: The NCEP/NCAR 40-Year Reanalysis Project. *Bull. Amer. Meteor. Soc.*, **77**, 437–472, doi:10.1175/1520-0477(1996)077<0437:TNYRP>2.0.CO;2.

Kirchner, I., G. L. Stenchikov, H.-F. Graf, A. Robock, and J. C. Antuña, 1999: Climate model simulation of winter warming and summer cooling following the 1991 Mount Pinatubo volcanic eruption. *J. Geophys. Res.*, **104**, 19 039–19 055, doi:10.1029/1999JD900213.

Krakauer, N. Y., and J. T. Randerson, 2003: Do volcanic eruptions enhance or diminish net primary production? Evidence from tree rings. *Global Biogeochem. Cycles*, **17**, 1118, doi:10.1029/2003GB002076.

Lau, K. M., and M. T. Li, 1984: The monsoon of East Asia and its global associations—A survey. *Bull. Amer. Meteor. Soc.*, **65**, 114–125, doi:10.1175/1520-0477(1984)065<0114:TMOEAA>2.0.CO;2.

Lean, J., J. Beer, and R. Bradley, 1995: Reconstruction of solar irradiance since 1610: Implications for climate change. *Geophys. Res. Lett.*, **22**, 3195–3198, doi:10.1029/95GL03093.

Li, F., and H. J. Wang, 2012: Predictability of the East Asian winter monsoon interannual variability as indicated by the DEMETER CGCMS. *Adv. Atmos. Sci.*, **29**, 441–454, doi:10.1007/s00376-011-1115-3.

Liu, F., J. Chai, G. Huang, J. Liu, and Z. Y. Chen, 2015: Modulation of decadal ENSO-like variation by effective solar radiation. *Dyn. Atmos. Oceans*, **72**, 52–61, doi:10.1016/j.dynatmoce.2015.10.003.

Liu, J. P., J. A. Curry, H. J. Wang, M. Song, and R. M. Horton, 2012: Impact of declining Arctic sea ice on winter snowfall. *Proc. Natl. Acad. Sci. USA*, **109**, 4074–4079, doi:10.1073/pnas.1114910109.

Maher, N., S. McGregor, M. H. England, and A. Sen Gupta, 2015: Effects of volcanism on tropical variability. *Geophys. Res. Lett.*, **42**, 6024–6033, doi:10.1002/2015GL064751.

Mantua, N. J., and S. R. Hare, 2002: The Pacific Decadal Oscillation. *J. Oceanogr.*, **58**, 35–44, doi:10.1023/A:1015820616384.

Mass, C. F., and D. A. Portman, 1989: Major volcanic eruptions and climate: A critical evaluation. *J. Climate*, **2**, 566–593, doi:10.1175/1520-0442(1989)002<0566:MVEACA>2.0.CO;2.

Mitchell, J. M., 1961: Recent secular changes of the global temperature. *Ann. N. Y. Acad. Sci.*, **95**, 235–250, doi:10.1111/j.1749-6632.1961.tb50036.x.

Mitchell, T. D., and P. D. Jones, 2005: An improved method of constructing a database of monthly climate observations and associated high-resolution grids. *Int. J. Climatol.*, **25**, 693–712, doi:10.1002/joc.1181.

Oman, L., A. Robock, G. Stenchikov, G. A. Schmidt, and R. Ruedy, 2005: Climatic response to high-latitude volcanic eruptions. *J. Geophys. Res.*, **110**, 2515–2530, doi:10.1029/2004JD005487.

Otterå, O. H., 2008: Simulating the effects of the 1991 Mount Pinatubo volcanic eruption using the ARPEGE atmosphere general circulation model. *Adv. Atmos. Sci.*, **25**, 213–226, doi:10.1007/s00376-008-0213-3.

——, M. Bentsen, I. Bethke, and N. G. Kvamstø, 2009: Simulated pre-industrial climate in Bergen Climate Model (version 2): Model description and large-scale circulation features. *Geosci. Model Dev.*, **2**, 197–212, doi:10.5194/gmd-2-197-2009.

——, ——, H. Drange, and L. L. Suo, 2010: External forcing as a metronome for Atlantic multidecadal variability. *Nat. Geosci.*, **3**, 688–694, doi:10.1038/ngeo955.

Perlwitz, J., and H.-F. Graf, 1995: The statistical connection between tropospheric and stratospheric circulation of the Northern Hemisphere in winter. *J. Climate*, **8**, 2281–2295, doi:10.1175/1520-0442(1995)008<2281:TSCBTA>2.0.CO;2.

Rind, D., J. Lean, and R. Healy, 1999: Simulated time-dependent climate response to solar radiative forcing since 1600. *J. Geophys. Res.*, **104**, 1973–1990, doi:10.1029/1998JD200020.

Robock, A., 1991: The volcanic contribution to climate change of the past 100 years. *Greenhouse-Gas-Induced Climatic Change: A Critical Appraisal of Simulations and Observations*, M. E. Schlesinger, Ed., Elsevier, 429–444.

——, 2000: Volcanic eruptions and climate. *Rev. Geophys.*, **38**, 191–219, doi:10.1029/1998RG000054.

——, and J. Mao, 1992: Winter warming from large volcanic eruptions. *Geophys. Res. Lett.*, **19**, 2405–2408, doi:10.1029/92GL02627.

——, and ——, 1995: The volcanic signal in surface temperature observations. *J. Climate*, **8**, 1086–1103, doi:10.1175/1520-0442(1995)008<1086:TVSIST>2.0.CO;2.

Salas Mélia, D., 2002: A global coupled sea ice–ocean model. *Ocean Modell.*, **4**, 137–172, doi:10.1016/S1463-5003(01)00015-4.

Sato, M., J. E. Hansen, M. P. McCormick, and J. B. Pollack, 1993: Stratospheric aerosol optical depths (1850–1990). *J. Geophys. Res.*, **98**, 22 987–22 994, doi:10.1029/93JD02553.

Schneider, D. P., C. M. Ammann, B. L. Otto-Bliesner, and D. S. Kaufman, 2009: Climate response to large, high-latitude and low-latitude volcanic eruptions in the Community Climate System Model. *J. Geophys. Res.*, **114**, D15101, doi:10.1029/2008JD011222.

Shindell, D. T., G. A. Schmidt, M. E. Mann, and G. Faluvegi, 2004: Dynamic winter climate response to large tropical volcanic

eruptions since 1600. *J. Geophys. Res.*, **109**, D05104, doi:10.1029/2003JD004151.

Stenchikov, G. L., I. Kirchner, A. Robock, H. F. Graf, J. C. Antuna, R. G. Grainger, A. Lambert, and L. Thomason, 1998: Radiative forcing from the 1991 Mount Pinatubo volcanic eruption. *J. Geophys. Res.*, **103**, 13 837–13 857, doi:10.1029/98JD00693.

——, T. L. Delworth, V. Ramaswamy, R. J. Stouffer, A. Wittenberg, and F. Zeng, 2009: Volcanic signals in oceans. *J. Geophys. Res.*, **114**, doi:10.1029/2008JD011673.

Stott, P. A., S. F. B. Tett, G. S. Jones, M. R. Allen, J. F. B. Mitchell, and G. J. Jenkins, 2000: External control of 20th century temperature by natural and anthropogenic forcings. *Science*, **290**, 2133–2137, doi:10.1126/science.290.5499.2133.

——, ——, ——, ——, W. J. Ingram, and J. F. Mitchell, 2001: Attribution of twentieth century temperature change to natural and anthropogenic causes. *Climate Dyn.*, **17**, 1–21, doi:10.1007/PL00007924.

Sun, J. Q., H. J. Wang, W. Yuan, and H. P. Chen, 2010: Spatial–temporal features of intense snowfall events in China and their possible change. *J. Geophys. Res.*, **115**, 751–763, doi:10.1029/2009JD012757.

Tan, B. K., L. L. Suo, and J. Y. Huang, 2007: Variability of coupling between surface air temperatures and northern annular modes at various levels. *Acta Meteor. Sin.*, **65**, 718–724.

Tao, S. Y., and L. X. Chen, 1987: A review of recent research on the East Asian monsoon in China. *Monsoon Meteorology*, C. P. Chang and T. N. Krishnamurti, Eds., Oxford University Press, 60–92.

Terray, L., and O. Thual, 1995: OASIS: Le couplage océan–atmosphère. *Meteorologie*, **10**, 50–61, doi:10.4267/2042/51962.

Trenberth, K. E., and A. Dai, 2007: Effects of Mount Pinatubo volcanic eruption on the hydrological cycle as an analog of geoengineering. *Geophys. Res. Lett.*, **34**, L15702, doi:10.1029/2007GL030524.

Wang, B., R. Wu, and X. Fu, 2000: Pacific–East Asian teleconnection: How does ENSO affect East Asian climate? *J. Climate*, **13**, 1517–1536, doi:10.1175/1520-0442(2000)013<1517:PEATHD>2.0.CO;2.

Wang, H. J., and D. B. Jiang, 2004: A new East Asian winter monsoon intensity index and atmospheric circulation comparison between strong and weak composite. *Quat. Sci.*, **24**, 19–27.

——, and K. Fan, 2005: Central-north China precipitation as reconstructed from the Qing dynasty: Signal of the Antarctic Atmospheric Oscillation. *Geophys. Res. Lett.*, **32**, L24705, doi:10.1029/2005GL024562.

——, and J. Q. Sun, 2009: Variability of Northeast China river break-up date. *Adv. Atmos. Sci.*, **26**, 701–706, doi:10.1007/s00376-009-9035-1.

——, and S. P. He, 2012: Weakening relationship between East Asian winter monsoon and ENSO after mid-1970s. *Chin. Sci. Bull.*, **57**, 3535–3540, doi:10.1007/s11434-012-5285-x.

——, and K. Fan, 2013: Recent changes in the East Asian monsoon (in Chinese). *Chin. J. Atmos. Sci.*, **37**, 313–318.

——, and Coauthors, 2012: Extreme climate in China: Facts, simulation and projection. *Meteor. Z.*, **21**, 279–304, doi:10.1127/0941-2948/2012/0330.

Wang, T., O. H. Otterå, Y. Q. Gao, and H. J. Wang, 2012: The response of the North Pacific Decadal Variability to strong tropical volcanic eruptions. *Climate Dyn.*, **39**, 2917–2936, doi:10.1007/s00382-012-1373-5.

——, H. J. Wang, O. H. Otterå, Y. Q. Gao, L. L. Suo, T. Furevik, and L. Yu, 2013: Anthropogenic agent implicated as a prime driver of shift in precipitation in eastern China in the late 1970s. *Atmos. Chem. Phys.*, **13**, 12 433–12 450, doi:10.5194/acp-13-12433-2013.

Wigley, T., P. Jones, and S. Raper, 1997: The observed global warming record: What does it tell us? *Proc. Natl. Acad. Sci. USA*, **94**, 8314–8320, doi:10.1073/pnas.94.16.8314.

Wu, B., and J. Wang, 2002: Winter Arctic Oscillation, Siberian High and East Asian winter monsoon. *Geophys. Res. Lett.*, **29**, 1897, doi:10.1029/2002GL015373.

Yan, H., W. Zhou, H. Yang, and Y. Cai, 2009: Definition of an East Asian winter monsoon index and its variation characteristics. *Trans. Atmos. Sci.*, **32**, 367–376.

Yang, S., and X. Jiang, 2014: Prediction of eastern and central Pacific ENSO events and their impacts on East Asian climate by the NCEP Climate Forecast System. *J. Climate*, **27**, 4451–4472, doi:10.1175/JCLI-D-13-00471.1.

——, K. M. Lau, and K. M. Kim, 2002: Variations of the East Asian jet stream and Asian–Pacific–American winter climate anomalies. *J. Climate*, **15**, 306–325, doi:10.1175/1520-0442(2002)015<0306:VOTEAJ>2.0.CO;2.

Zanchettin, D., C. Timmreck, H.-F. Graf, A. Rubino, S. Lorenz, K. Lohmann, K. Kruger, and J. Jungclaus, 2012: Bi-decadal variability excited in the coupled ocean–atmosphere system by strong tropical volcanic eruptions. *Climate Dyn.*, **39**, 419–444, doi:10.1007/s00382-011-1167-1.

——, ——, O. Bothe, S. J. Lorenz, G. Hegerl, H.-F. Graf, J. Luterbacher, and J. H. Jungclaus, 2013: Delayed winter warming: A robust decadal response to strong tropical volcanic eruptions? *Geophys. Res. Lett.*, **40**, 204–209, doi:10.1029/2012GL054403.

Zhou, Q., W. Chen, and W. Zhou, 2013: Solar cycle modulation of the ENSO impact on the winter climate of East Asia. *J. Geophys. Res.*, **118**, 5111–5119, doi:10.1002/jgrd.50453.

Zhou, W., X. Wang, T. J. Zhou, C. Y. Li, and J. C. L. Chan, 2007: Interdecadal variability of the relationship between the East Asian winter monsoon and ENSO. *Meteor. Atmos. Phys.*, **98**, 283–293, doi:10.1007/s00703-007-0263-6.

Zhu, Y., H. Wang, W. Zhou, and J. Ma, 2011: Recent changes in the summer precipitation pattern in East China and the background circulation. *Climate Dyn.*, **36**, 1463–1473, doi:10.1007/s00382-010-0852-9.